# A deformation mechanism map for IN738LC superalloy

J. A. CAREY, P. M. SARGENT, D. R. H. JONES
*Department of Engineering, University of Cambridge, Trumpington Street, Cambridge CB2 1PZ, UK*

The development of complex high-temperature alloys has been a major factor in the great increases in efficiency and thrust that have been obtained from gas turbine engines since their invention. Since 1971, as part of the continuing agreements on Collaboration in Science and Technology (COST), several countries have co-operated in the research and development of such high-temperature alloys. Project COST-50 began in 1973 and consisted of 60 concerted programmes of research [1, 2]. In particular, directional solidification (DS) methods have been developed for the alloy IN738LC [3]. Preliminary results for DS alloys had indicated superior creep rupture properties compared with conventionally cast (OC) alloys [4–6]. This letter reports new data on the isothermal creep properties of the DS alloy IN738LC, which is used as a blading material for the first-row high-pressure stage of gas turbines [7].

The following nomenclature is used:

| | |
|---|---|
| $A$ | Dorn constant |
| $b$ | Burgers vector |
| $b_b$ | Burgers vector for grain boundary dislocations (approximately $b/3$) |
| $C$ | dimensionless constant (approximately 40) |
| $D_{0v}$ | pre-exponential term for lattice vacancy diffusion |
| $d$ | grain size |
| $\Delta F$ | activation energy for glide |
| $k$ | Boltzmann's constant |
| $L$ | spacing of obstacles in grain boundary |
| $n$ | stress exponent for power-law creep |
| $Q_{crp}$ | activation energy for power-law creep |
| $Q_v$ | activation energy for lattice vacancy diffusion |
| $R$ | gas constant |
| $T$ | absolute temperature |
| $T_m$ | absolute melting temperature |
| $\dot{\gamma}$ | shear strain rate |
| $\mu$ | shear modulus |
| $\mu_T$ | shear modulus at absolute temperature $T$, e.g. $\mu_0$ at 0 K, $\mu_{300}$ at 300 K |
| $\sigma_0$ | pre-exponent for obstacle-controlled glide |
| $\sigma_s$ | applied shear stress |
| $\sigma_t$ | threshold stress |
| $\Omega$ | atomic volume |

Figs 1 and 2 show deformation maps for IN738LC constructed according to the methods described by Frost and Ashby [8]. They are based on the DS data plotted on the maps and on the parameters listed in Table I. The stress–temperature map shows only the high-temperature, high-stress region, in order to display the experimental results more clearly. The strain rate–stress map shows that the full range of data does not exactly fit the power-law description in that the stress exponent is lower at low stresses and higher at high stresses than would be expected. In the construction of the maps the applied stress is presented as the equivalent shear stress normalized with respect to the shear modulus [8]. The stress-rupture data give only an upper-bound on the "steady-state" strain rate and so fit the predicted contours on both maps only approximately.

Samples were prepared at the National Physical Laboratory (NPL) under the guidance of Drs Quested and McLean. IN738LC barstock as supplied by Henry Wiggin and Co. was cleaned and remelted in a high-vacuum furnace. After casting, a single rod was directionally solidified at 300 mm $h^{-1}$ using a modified Bridgeman apparatus incorporating a molten Woods-metal bath to assist heat loss. Transverse and longitudinal metallographic sections were prepared to ensure that the directional solidification had been successful. In general the microstructure was similar to that observed by other workers for this and related alloys [3, 4, 9–14], except that some carbide precipitation was observed, as reported previously for Inconel 617 and MAR-M200 [4, 13].

TABLE I Material data for IN738LC

| | | Notes |
|---|---|---|
| Crystallographic and thermal | | |
| $\Omega$ ($m^3$) | $1.1 \times 10^{-29}$ | (a) |
| $b$ (m) | $2.5 \times 10^{-10}$ | (a) |
| $T_m$ (K) | 1500 | (b) |
| Shear modulus | | |
| $\mu_{300}$ (MPa) | $8.0 \times 10^4$ | (a) |
| $(d\mu/dT)$ $(T_m/\mu_{300})$ | −0.5 | (a) |
| Lattice vacancy diffusion | | |
| $D_{0v}$ ($m^2$ $sec^{-1}$) | $2.0 \times 10^{-4}$ | (c) |
| $Q_v$ (kJ $mol^{-1}$) | 285 | (a) |
| $\sigma_t/\mu$ | $2.0 \times 10^{-4}$ | (d) |
| Power-law creep | | |
| $n$ | 7.7 | (e) |
| $A$ | $5.8 \times 10^{12}$ | (c) |
| $Q_{crp}$ (kJ $mol^{-1}$) | 512 | (f) |
| Obstacle-controlled glide | | |
| $\sigma_s/\mu_0$ | $7.6 \times 10^{-3}$ | (g) |
| $\dot{\gamma}$ ($sec^{-1}$) | $1.0 \times 10^6$ | (a) |
| $\Delta F/\mu_0 b^3$ | 2.0 | (a) |

[a] See [8], p. 54. Data for MAR-M200.
[b] Solidus temperature.
[c] Value obtained by fitting experimental data to Equations 1 and 2 as appropriate.
[d] See text.
[e] See text and Fig. 4.
[f] See text and Fig. 3.
[g] See [7].


0261–8028/90 $03.00 + .12 

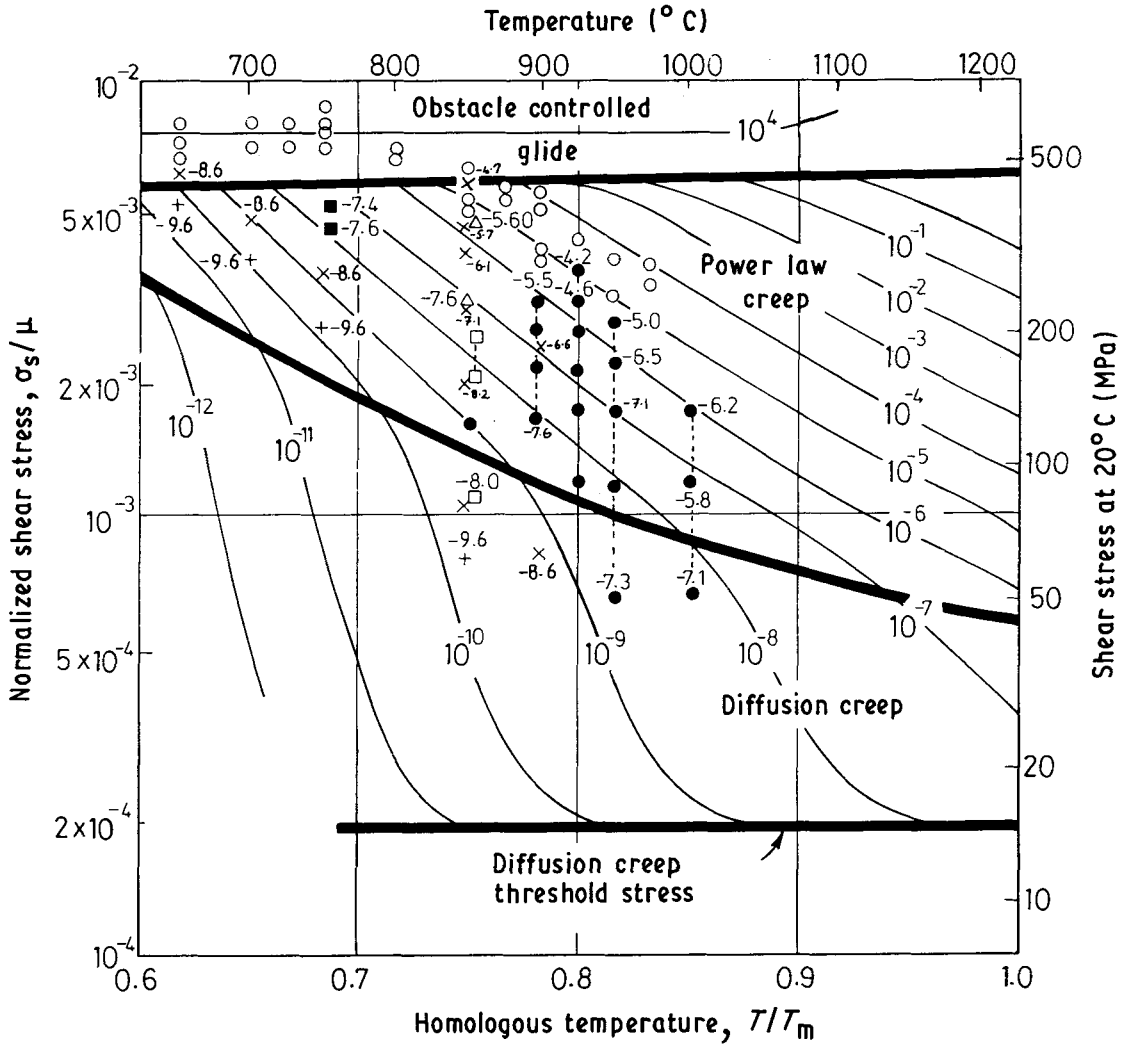


*Figure 1* A stress–temperature deformation mechanism map for IN738LC with an average grain size of 0.3 mm. Contours of strain rate are in $sec^{-1}$. (■) [12], (△) [10] DS, (□, ●) [7] CC and DC, respectively, (○, ×, +) [8] yield, $10^4$ h rupture and $10^5$ h rupture, respectively.

Isothermal creep measurements were made with a 15 : 1 lever-arm rig and a conventional resistance heater using tensile stresses between 50 and 450 MPa. The temperature variation along the gauge length was within $\pm 3°$ C and the furnace was kept within $\pm 2°$ C for periods of up to 5 days. The minimum strain rate resolution was approximately $10^{-8}\,sec^{-1}$ and the cumulative plastic strain arising from each test was less than 4%, so that all can be regarded as "constant stress' tests. Further details of the experimental techniques used were described by Carey [7].

The major elements in solid solution affect the crystallographic data, the shear modulus and the dependence of the shear modulus on temperature, but these properties are largely independent of microstructure. Therefore values are taken from similar superalloys as reported by Frost and Ashby [8].

In order to estimate the activation energy for creep, an Arrhenius relationship was assumed between tensile strain rate and temperature. Fig. 3 shows that this asumption is justified, and from it a value of $512\,kJ\,mol^{-1}$ was obtained. In normalized terms this is $41RT_m$, very high for a pure metal or substitutional alloy, but similar to other observations for particle-and-precipitate reinforced alloys [14].

The stress exponent for power-law creep was determined for DS IN738LC using the data in Fig. 4. The results compare well with previously published data, despite differences in heat treatment, and there is excellent agreement with Quested's DS data for material produced using the same drawing conditions. However, there appears to be little overall difference between the creep rates for DS and OC specimens, although the ductility and creep life for the DS material are superior [7]. The value of 7.7 for $n$ is the same as that measured for MAR-M200 [14].

In the construction of the maps the constitutive equation

$$\dot{\gamma} = A(\mu_T b/kT)\,(\sigma_s/\mu)^n \exp(-Q_{crp}/RT) \quad (1)$$

was used.

At relatively high temperatures and low stresses there is significant disagreement between the data and the predictions of the maps. The increase in creep rate has previously been attributed to coarsening of the gamma-prime phase [11] but it may also be due, at least in part, to compositional changes which have been shown to occur in aligned primary dendrites in DS specimens [10]. In the present case, above about 1300 K, the gamma-prime phase in IN738 dissolves.

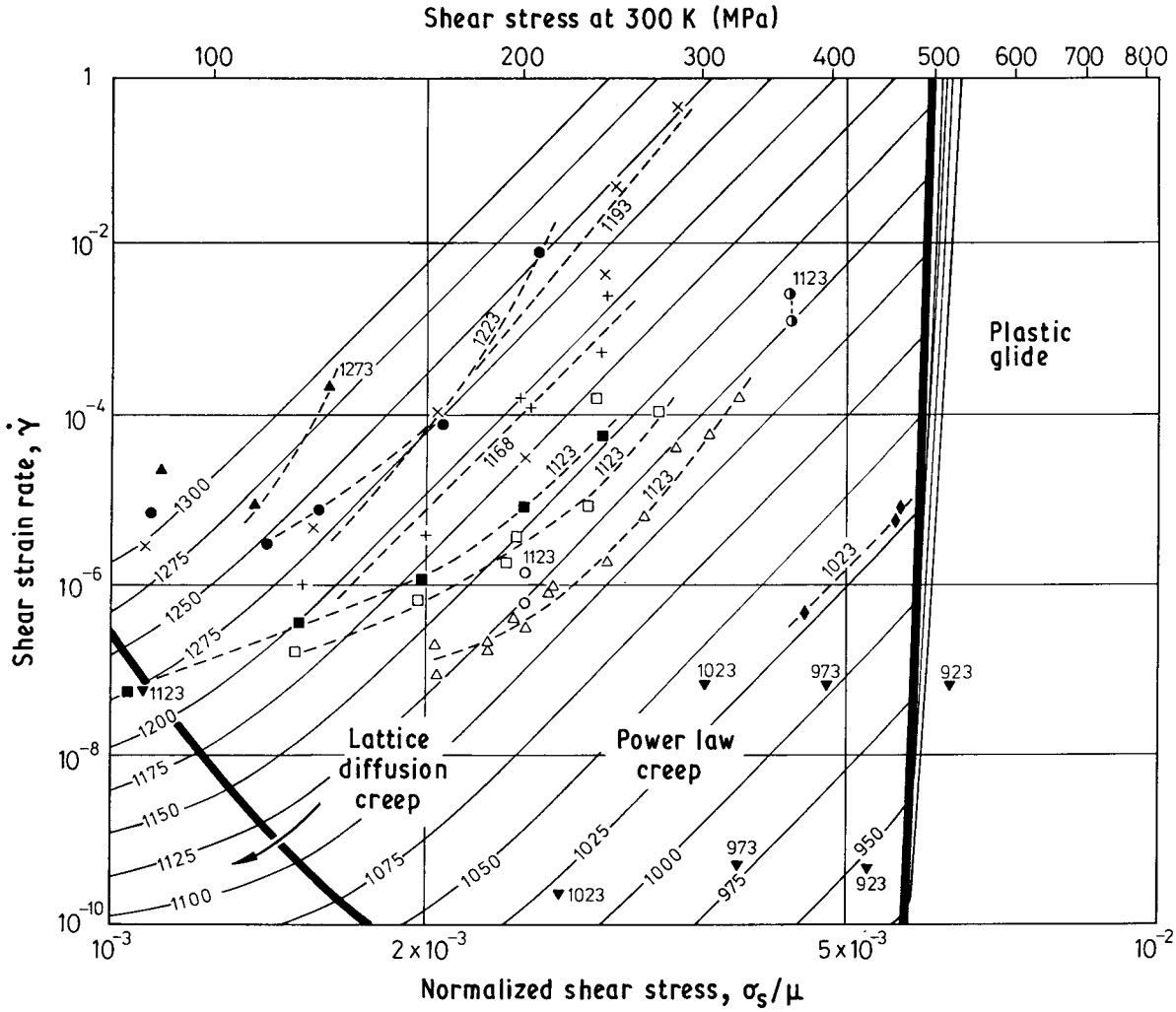


*Figure 2* A strain rate–stress deformation mechanism map for IN738LC with an average grain size of 0.3 mm. Contours of temperature are in K. (□, ●, ×, +, ▲) [7] DS, (■) [7] CC, (△) [11] CC + HT, (○, ◑) [10] DS and DS + HT, respectively, (▼) [8] rupture, (◆) [12] DS.

At slightly higher temperatures so do the carbides, whence the alloy will behave as a solid solution and dynamic recrystallization can be expected to occur. The contours on the stress–temperature map (Fig. 1) are therefore not useful predictions above about 1300 K. The strain rate–stress map (Fig. 2) is limited to temperatures below 1300 K, so the data contained there are not affected by these compositional changes.

The activation energy for diffusive creep is assumed to be similar to that of nickel in MAR-M200 and similar alloys (285 kJ mol$^{-1}$) as quoted by Frost and

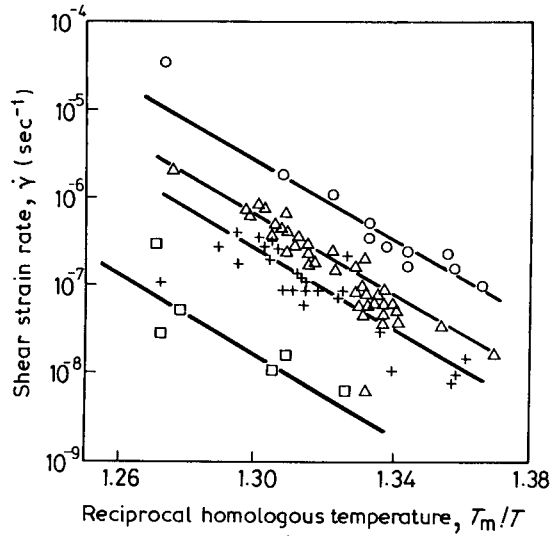


*Figure 3* Arrhenius plots of results for IN738LC. The activation energy for creep was determined from the slopes of the lines. (○) 336, (△) 289, (+) 241 and (□) 199 MPa.

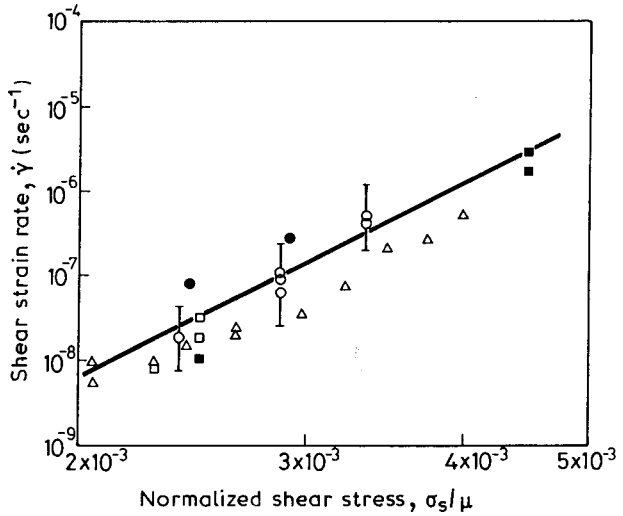


*Figure 4* Selected results for IN738LC plotted as shear strain rate against normalized shear stress ($\sigma_s/\mu$). The value of the power-law exponent was determined from the slope of the line. (○, ●) [7] AS and CC, respectively, (□, ■) [10] DS and DS + HT, respectively, (△) [11] CC + HT.

Ashby [8]. In normalized terms this is $23\,RT_m$, which is higher than the value of $18RT_m$ which is usually found for face-centred cubic solid-solution alloys [15]. The following constitutive equation was used for lattice creep on the maps:

$$\dot{\gamma} = (C/d^2)\sigma_s(\Omega/kT)D_{0v} \exp(-Q_v/RT) \quad (2)$$

For a DS alloy the appropriate grain size in this equation is the mean distance that a diffusing vacancy has to travel to find a sink on an interface in tension. In the case of a DS alloy this is the length of the grain along the solidification direction, which is 0.3 mm in the present case.

The assumed threshold stress is that expected for particle-strengthened alloys where diffusive creep cannot occur if vacancies cannot be absorbed at particle–matrix interfaces. This is because the present stresses are too low for grain-boundary dislocation glide [16]. The threshold stress may be written as

$$\sigma_t \approx \mu b_b/L \quad (3)$$

If $L$ is the spacing of the gamma-prime precipitates, which is about 500 nm [11], then using the data in Table I we obtain a value for $\sigma_t/\mu$ of about $2 \times 10^{-4}$.

This diffusion-creep threshold must be distinguished from the threshold stress for power-law creep. The latter is affected by the particle spacing in the body of the grains, and this is thought to be the reason why stress exponents for superalloys (7.7 in the case of IN738LC) are greater than the theoretically predicted value of 3 [17].

To summarize, new data for OC and DS IN738LC have been combined with data from the literature to construct high-temperature deformation mechanism maps for the alloys. These show a high-stress plasticity regime controlled by dislocation glide, a power-law creep field and a strong indication of a vacancy-diffusion creep field at low stresses. No evidence was found for a grain-boundary diffusion creep field, but the curvature of the temperature contours at high stress (Fig. 2) could be due to a low-temperature dislocation-core diffusion-controlled power-law creep field, or to power-law breakdown, or to both. The vacancy-diffusion creep field is important because extrapolating power-law creep data to low stresses would severely underestimate the likely creep strain over the life of an engineering component.

Finally, deformation maps are a useful means of presenting data which span a wide range of experimental conditions, especially where they must be compared with existing results. The derivation of parameters from the data to ensure that a mechanism transition occurs in the predicted contours at the same place that it is observed (as in Fig. 2) puts extra bounds on the analysis of results that are not seen if the two mechanisms are fitted separately.

## Acknowledgements

The authors thank the NPL for supplying data in advance of publication and the Science and Engineering Research Council for supporting this research.

## References

1. D. COUTSOURADIS, P. FELIX, H. FISCHEMEISTER, L. HABRAKEN, Y. LINDBLOM and M. O. SPIEDEL (editors), "High Temperature Alloys for Gas Turbines" (Applied Science, London, 1978).
2. B. BUCHMEYR and H. KROCKEL, in COST-50 and COST-51 Conference on High-Temperature Alloys for Gas Turbines and Other Applications, Liège, October 1986.
3. M. McLEAN and F. SCHUBERT, in "High Temperature Alloys for Gas Turbines", edited by D. Coutsouradis, P. Felix, H. Fischmeister, L. Habraken, Y. Lindblom and M. O. Spiedel (Applied Science, London, 1978).
4. G. A. WEBSTER and J. J. PIEARCEY, *Trans. ASM* **59** (1966) 847.
5. F. L. VERSNYDER and M. E. SCHANK, *Mater. Sci. Eng.* **6** (1970) 213.
6. D. A. WOODFORD, *Met. Trans* **12A** (1981) 299.
7. J. A. CAREY, PhD dissertation, University of Cambridge (1983).
8. H. J. FROST and M. F. ASHBY, "Deformation-Mechanism Maps" (Pergamon Press, Oxford, 1982).
9. S. N. TEWARI, *Met. Trans.* **7A** (1976) 1237.
10. M. McLEAN and P. QUESTED, in "Creep and Fracture of Engineering Materials and Structures", edited by B. Wilshire and P. Owen (Pineridge Press, Engand, 1981).
11. R. A. STEVENS and P. E. J. FLEWITT, *Mater. Sci. Eng.* **50** (1981) 271.
12. P. J. HENDERSON and M. McLEAN, *Acta Metall.* **30** (1982) 1121.
13. S. KIHARA, J. B. NEWKIRK, A. OHTOMA and Y. SAIGA, *Met. Trans.* **11A** (1980) 1019,
14. G. A. WEBSTER and J. J. PIEARCEY, *J. Mater. Sci.* **1** (1967) 97.
15. A. BROWN and M. F. ASHBY, *Acta Metall.* **28** (1980) 1085.
16. E. ARZT and M. F. ASHBY, *Scripta Metall.* **16** (1982) 1285.
17. B. DERBY and M. F. ASHBY, *ibid.* **18** (1984) 1079.

*Received 21 August*
*and accepted 14 September 1989*